Precision Measurement of Transition Matrix Elements via Light Shift Cancellation

C. D. Herold,[*] V. D. Vaidya, X. Li, S. L. Rolston, and J. V. Porto

Joint Quantum Institute, University of Maryland and NIST, College Park, Maryland 20742, USA

M. S. Safronova

Department of Physics and Astronomy, University of Delaware, Newark, Delaware 19716, USA
(Received 20 August 2012; published 14 December 2012)

We present a method for accurate determination of atomic transition matrix elements at the 10^{-3} level. Measurements of the ac Stark (light) shift around "magic-zero" wavelengths, where the light shift vanishes, provide precise constraints on the matrix elements. We make the first measurement of the $5s - 6p$ matrix elements in rubidium by measuring the light shift around the 421 and 423 nm zeros through diffraction of a condensate off a sequence of standing wave pulses. In conjunction with existing theoretical and experimental data, we find $0.3235(9)ea_0$ and $0.5230(8)ea_0$ for the $5s - 6p_{1/2}$ and $5s - 6p_{3/2}$ elements, respectively, an order of magnitude more accurate than the best theoretical values. This technique can provide needed, accurate matrix elements for many atoms, including those used in atomic clocks, tests of fundamental symmetries, and quantum information.

Precise knowledge of atomic transition strengths is important in many current areas of research, including the development of ultraprecise atomic clocks [1–3], studies of fundamental symmetries [4,5] and degenerate quantum gases [6], quantum information [7,8], plasma physics [9], and astrophysics [10,11]. For example, one of the largest contributions to the uncertainty budget of atomic clocks is the uncertainty in the blackbody radiation (BBR) shift [2,12]. The BBR shift is calculated from the difference in the electric-dipole polarizabilities between the clock states [13], and its accuracy is currently limited by uncertainty in atomic transition matrix elements. The dynamic correction to the BBR shift can also be determined accurately if the relevant matrix elements are known [1]. Studies of fundamental symmetries, such as atomic parity violation, need transition matrix elements to evaluate parity-violating amplitudes and vector transition polarizabilities [4,5]. Accurate atomic theory can also be indispensable to the design and interpretation of experiments, where direct measurement of all relevant parameters is infeasible. More complicated atoms, such as Er [14], Dy [15], and Ho [16] have recently become of interest, and development of new theoretical methods must be supported by the existence of high-precision experimental benchmarks.

Transition matrix elements can be difficult to measure or calculate accurately. State-of-the-art theory predictions are often limited to a few percent uncertainty, and the presently available experimental techniques typically measure matrix elements accurately only for one or two of the lowest transitions. To date, the most accurate determinations of atomic transition matrix elements are through excited state lifetime measurements or photoassociation spectroscopy [17]. The former is limited by uncertainty in branching ratios when multiple decay paths exist. As a result, although the $6p$ lifetime of rubidium was measured to 1%, no matrix elements were reported [18]. The latter requires species with purely long-range molecular excited states where molecular theory is sufficiently well known to extract atomic properties. In principle, transition matrix elements can be determined from the ac polarizability α by measuring the ac Stark (light) shift of an atom exposed to light of known intensity. However, unlike dc Stark shift measurements, where the applied electric field can be determined geometrically [2], it is difficult to accurately determine the optical intensity, limiting the efficacy of this approach. (Lifetime measurements avoid this calibration challenge by using a well known field, the vacuum.) For atoms with spin-dependent vector light shifts and two long-lived states, rf spectroscopy was used to accurately determine the *ratio* of two vector light shifts [19,20], which when combined with theory constrained matrix elements [21]. New techniques are needed to improve accuracy, extend the range of measurable matrix elements, and provide benchmarks for theory.

In this Letter, we present a widely applicable method, recently suggested in Ref. [22], for constraining matrix elements at the 10^{-3} level through direct measurement of light shifts near magic-zero wavelengths (λ_{zero}), where the combined light shift from all transitions cancels [23]. These λ_{zero} wavelengths are distinct from the "magic" wavelengths used in optical clocks, where the light shift is identical for two states [24]. We measure small light shifts through diffraction off a standing wave, amplifying the diffracted populations by constructively interfering the effect of up to $n_p = 15$ pulses, resulting in an n_p^2 enhancement in the diffracted fraction. We make the first experimental determination of the rubidium $5s - 6p_{1/2}$ and $5s - 6p_{3/2}$ electric dipole matrix elements, to an accuracy

of 0.3%, 10 times more accurate than the best theoretical values [22]. Implementation of our measurement technique could provide much-needed data to constrain the BBR shift for optical lattice clocks.

Measuring light shifts near a λ_{zero} to constrain matrix elements has a number of advantages over the approaches described earlier. It is insensitive to absolute calibration of the applied optical field, requiring only a stable intensity. Scalar light shifts are present for all atomic states, and λ_{zero} points are found near every atomic transition. That proximity increases sensitivity to the matrix element of the nearby transition in addition to decreasing sensitivity to uncertainty in hard-to-calculate theoretical values. Most importantly, ground (or metastable) state light shifts depend only on matrix elements directly to higher excited states, not on the coupling of the excited states to other states. Light shift measurements are thus independent of the branching ratios that limit the lifetime approach.

We used this technique to measure the transition matrix elements between the ground $5s_{1/2}$ and $6p_{1/2}$, $6p_{3/2}$ states in ^{87}Rb by measuring the light shift as a function of λ near the two λ_{zero} points neighboring the $6p$ states (see the inset in Fig. 1). We applied a sequence of standing wave (optical lattice) pulses to a Bose-Einstein condensate (BEC) containing $\simeq 3.5 \times 10^4$ $|F = 1, m_F = -1\rangle$ atoms with no discernible thermal fraction, produced in a hybrid optical and magnetic trap similar to Ref. [25]. At the end of the pulse sequence, we suddenly turn off the trap and measure the atom population in each diffracted order from an absorption image after 40 ms time of flight. By intentionally using a small condensate, we can neglect atom-atom interactions and limit the optical depth so that all orders in the image are unsaturated. The measured population fractions, normalized to the total number in each image, are insensitive to small fluctuations in total atom number.

The lattice light is provided by a frequency-doubled diode laser and is tunable between 419 and 424 nm. We measure the wavelength to 50 fm (90 MHz) accuracy with a
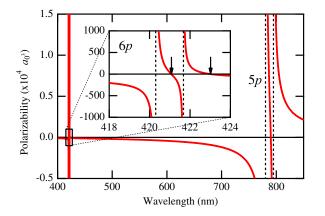

FIG. 1 (color online).   Calculated polarizability of Rb (atomic units of a_0^3). The vertical dashed lines are at the np-$5s$ transitions. Arrows indicate the positions of the relevant λ_{zero} points.

wave meter, calibrated to the known $5s - 6p$ transition frequencies [26]. We form the lattice by reimaging a retro-reflected beam on the atoms with an incident power of 60–120 mW and a waist of $\simeq 110$ μm. The lattice beam intensity varies only a few percent across the BEC, whose Thomas-Fermi radius is 18 μm transverse to the beam. Lattice alignment is performed at 421.700 nm where the light shift is reasonably large, $\simeq 7E_R$ [where the recoil energy $E_R = \hbar^2 k^2/(2M)$ for wave vector $k = 2\pi/\lambda$, lattice laser wavelength λ, and atomic mass M]. The input beam is carefully aligned to the BEC (with the retroreflected beam blocked) by minimizing the transverse displacement of the BEC induced by the beam. The retroreflected beam is then aligned by maximizing diffraction efficiency. Lattice depth measurements at the 5% uncertainty level are consistent with no drift during a data set, and the alignment is typically stable from day to day.

To minimize wavelength-dependent steering of the laser, we couple the light through an optical fiber and focus the output of the fiber onto the BEC. We measured the residual steering after the fiber by monitoring the position of the beam 1 m downstream from the fiber tip. The observed deflection of the beam was <30 μrad, which corresponds to at worst a 1% decrease in average beam intensity at the BEC and is included in our uncertainty analysis. Additionally, we monitor the power in each pulse sequence with a photodiode to account for different laser powers.

Lattice polarization also affects the measured light shift. Linearly polarized light has a nearly scalar light shift [27], but elliptical polarization will have both vector and scalar light shifts for atoms with $|m_F| > 0$ [28], shifting the position of λ_{zero}. Although we used a Glan-laser polarizer to establish a clean linear polarization, analyzing the light after the chamber showed that the vacuum windows' slight birefringence created $\simeq 1\%$ ellipticity. To account for the possible systematic shift of λ_{zero}, we measured the light shift for two orthogonal, linear input polarizations, defined as S and P with respect to the plane of the last mirror before the chamber. By symmetry, the induced ellipticity from the window is opposite for the two input polarizations. We calculated that averaging the S and P measurements cancels the contribution of the vector light shift to a negligible 10 fm shift in λ_{zero}.

Optical lattice depths (light shifts) are commonly measured by observing the population oscillations between momenta $2l\hbar k$, for integer l, as a function of lattice pulse duration (outside the Raman-Nath regime). For lattice depths below $1E_R$, the diffracted populations are small, and the oscillation period saturates to $h/(4E_R)$. At $0.05E_R$, less than 0.008% of atoms are diffracted for a single lattice pulse. In order to increase the signal, we employ a multipulse diffraction sequence that coherently adds the effect of each pulse, similar to quantum resonances in delta-kicked rotors [29,30]. For weak lattices where only orders with $|l| \leq 1$ are populated, a Bloch sphere picture

provides intuition [31] (Fig. 2). For initially stationary atoms, the $|l| = 1$ orders are equivalent and can be represented as a single state, which along with the $l = 0$ state are the two poles of the Bloch sphere. Free evolution corresponds to precession about the vertical axis with period $h/(4E_R)$, called the Talbot time [32]. During a weak lattice pulse, the precession axis is tilted by an angle proportional to the lattice depth with essentially the same $h/(4E_R)$ period [33]. Alternating lattice and free evolution with duration $h/(8E_R)$ (one-half precession period, $\simeq 9.75$ μs at 423 nm) efficiently increases the diffracted population (see Fig. 2).

To accurately determine the lattice depths from the measured populations, we numerically diagonalized the lattice Hamiltonian (see, e.g., Ref. [31]) in the plane wave basis including orders up to $|l| = 3$. From this we calculate the first-order diffracted population fraction P_1 as a function of pulse number n_p and lattice depth V_0 in units of E_R. In the weakly diffracting limit ($n_p V_0 \ll 4$), $P_1 \propto (n_p V_0)^2$, showing that multiple weak pulses are equivalent to one pulse n_p times stronger. Inverting the numeric result for P_1, we extract the lattice depth $V_0(n_p, P_1)$ from the measured population fraction $P_1 = (N_{-1} + N_1)/N_{\text{tot}}$, with N_l the number of atoms in the lth order. Figure 3 shows P_1 versus n_p at fixed V_0. The agreement with theory is excellent for n_p up to 18. We attribute deviations at larger n_p to the reduced overlap of the diffracted components, which travel a significant fraction of the size of the BEC, during the pulse sequence.

To determine the polarizability α, we extract the raw lattice depth $V_0(n_p, P_1)$ for each image, which is then divided by the measured photodiode power for that pulse
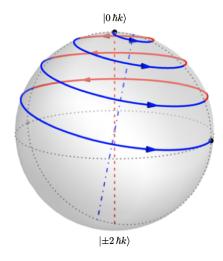

$|0\,\hbar k\rangle$

$|\pm 2\,\hbar k\rangle$

FIG. 2 (color online). A Bloch sphere representation of the state vector's evolution during a pulse sequence. The state vector starts in $|0\hbar k\rangle$ (north pole). Lattice (free) evolution is shown in blue (red). Alternating lattice and free evolutions with duration $h/(8E_R)$, the diffracted population is maximized as described in the text. This sequence provides 50% population in $|\pm 2\hbar k\rangle$ after four pulses, corresponding to a lattice depth of $\simeq 1E_R$, much larger than depths we actually measured.

sequence. Although this gives $|\alpha|$, theory is sufficiently accurate to unambiguously choose the sign. Figure 4 shows the extracted polarizability as a function of λ for four data sets: two orthogonal polarizations, S and P, near each λ_{zero}. The lattice is aligned before each data set, and measurements after confirm consistent alignment within a data set. The measurement is repeated up to 20 times at each wavelength [34], and the error bars in Fig. 4 represent purely statistical uncertainty of 1σ. For both sets around the 421 nm zero, we used 15 pulses, and for both sets around 423 nm we used 8 or 11 pulses.

We fit the polarizability to the expression calculated in [22]:

$$\alpha \propto \frac{1}{3} \sum_{n=5}^{8} \sum_{j=1/2}^{3/2} \frac{|d_{np_j}|^2 \omega_{np_j}}{\omega^2 - \omega_{np_j}^2} + C_{\text{tail}} + C_{\text{core}}, \qquad (1)$$

where the $d_{np_j} \equiv \langle np_j \| D \| 5s \rangle$ are reduced dipole matrix elements and ω is the lattice laser frequency. The matrix elements $d_{6p_{1/2}}$ and $d_{6p_{3/2}}$ are fit parameters, while $d_{5p_{1/2}}$ and $d_{5p_{3/2}}$ are fixed by the experimental lifetime measurement [35]. The $7p$ and $8p$ matrix elements and the contribution C_{core}, which includes the polarizability of the core electrons and their interaction with the valence electron, are calculated in Ref. [22]. We used an improved calculation of C_{tail}, the valence contribution for $n > 8$, with reduced uncertainty (see Supplemental Material [36]).

Fitting the data to Eq. (1) around a given λ_{zero} constrains the relationship among the parameters in the equation. For example, the position of the λ_{zero} near 421 nm, which is between the two $6p$ lines, depends strongly on the *ratio* of the $6p$ matrix elements, $R_{6p} = d_{6p_{3/2}}/d_{6p_{1/2}}$, but more weakly on their absolute value. On the other hand, the position of the λ_{zero} near 423 nm, which is red-detuned of both $6p$ lines, depends more on the average value of the $6p$ elements (in relation to the $5p$ elements). Fits around a single λ_{zero} constrain $6p$ elements with respect to the non-$6p$ parameters (d_{np}, C_{tail}, and C_{core}), and the extracted values are sensitive to their uncertainties. Including data
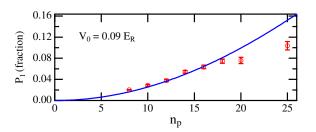

FIG. 3 (color online). Diffracted population at fixed laser power and wavelength. As we vary the number of pulses, the diffracted population (our signal) initially increases as n_p^2. The solid line is the theoretical calculation with only V_0 as a fit parameter. For accurate light shift measurements, we used only $n_p \lesssim 15$.
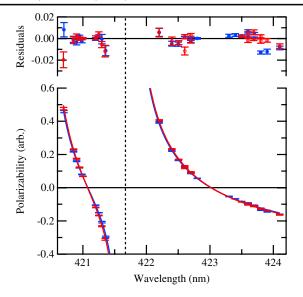
FIG. 4 (color online). Measured polarizability (arbitrary units) versus wavelength for two linear, orthogonal input polarizations S (red, open circles) and P (blue, filled circles). Each point is an average of up to 20 measurements, shown with 1σ statistical error bars. The solid lines (nearly indistinguishable) are fits to the expected form [Eq. (1)] with the $6p$ matrix elements as free parameters; reduced χ^2 for the S and P fits is 4 and 11, respectively [37]. Additionally, we allow a separate amplitude about each zero to account for different laser power. Fit residuals are shown at the top.

TABLE I. Absolute uncertainty contributions (in $ea_0 \times 10^{-4}$) for the $5s$-$6p$ matrix elements and their ratio ($\times 10^{-4}$). Note the insensitivity of R_{6p} to uncertainty in the fit parameters. Total uncertainty is summed in quadrature. Additionally, our $5s$-$6p$ matrix elements are compared to the theoretical values (in ea_0).

Contribution	$\delta d_{6p_{1/2}}$	$\delta d_{6p_{3/2}}$	δR_{6p}
Statistical	1.79	1.90	11.1
$d_{5p_{1/2}}$	0.84	1.34	0.004
$d_{7p_{1/2}}$	0.08	0.13	0.012
$d_{8p_{1/2}}$	0.02	0.04	0.003
$np_{1/2}$ tail	0.56	0.92	0.029
$d_{5p_{3/2}}$	1.77	2.87	0.007
$d_{7p_{3/2}}$	0.22	0.36	0.031
$d_{8p_{3/2}}$	0.06	0.10	0.007
$np_{3/2}$ tail	2.01	3.28	0.104
Core	1.25	2.05	0.064
Alignment drift	7.82	6.18	19.9
Total	8.62	8.24	22.8
Theoretical value [22]	0.325(9)	0.528(13)	1.624(7)
Our results	0.3235(9)	0.5230(8)	1.617(2)

around multiple λ_{zero} points further constrains the fits. For our case, where the two λ_{zero}'s are close to each other, the effect of the non-$6p$ contributions is essentially identical for the two zeros, so that simultaneous fits to both zeros accurately determine R_{6p}, independent of the other parameters. With the addition of sufficiently accurate theoretical and experimental values for the other d_{np}, C_{tail}, and C_{core}, we can also accurately determine absolute values for $d_{6p_{1/2}}$ and $d_{6p_{3/2}}$.

We simultaneously fit the 421 and 423 nm data sets for a given polarization. Because of possible differences in alignment and total power between sets, we fit with an independent amplitude A_λ around each λ_{zero} giving a total of four fit parameters: A_{421}, A_{423}, $d_{6p_{1/2}}$, and $d_{6p_{3/2}}$. The fit values are then averaged for the two polarizations. (The small difference in extracted matrix elements for S and P polarization is consistent with the 1% ellipticity discussed earlier.) Table I summarizes the contributions to our final uncertainty in our measured values for R_{6p}, $d_{6p_{1/2}}$, and $d_{6p_{3/2}}$. The statistical uncertainties in R_{6p}, $d_{6p_{1/2}}$, and $d_{6p_{3/2}}$ are roughly the same, of the order of 0.1%. As expected, the contribution of the uncertainties of the other fixed parameters in Eq. (1) to R_{6p} is negligible, providing a good comparison with theory, which can predict ratios more accurately than matrix elements (see Supplemental Material [36]). The uncertainties in $d_{6p_{1/2}}$ and $d_{6p_{3/2}}$ do

depend on the other parameters, and the two largest contributions are from the theoretical uncertainty in the $np_{3/2}$ component of C_{tail} and the experimental uncertainty in $d_{5p_{3/2}}$; these contribute at the 0.06% level. To account for potential lattice alignment drift, we simulated the effect of a 5% linear drift in the extracted polarizability across a data set, which resulted in an additional 0.2% uncertainty in $d_{6p_{1/2}}$ and 0.1% in R_{6p} and $d_{6p_{3/2}}$ [37].

Our light shift cancellation measurement technique accurately determines the ratio of the $6p$ matrix elements, with $R_{6p} = 1.617(2)$. The matrix elements are $d_{6p_{1/2}} = 0.3235(9)$ and $d_{6p_{3/2}} = 0.5230(8)$, in excellent agreement with the theoretical values (Table I). From these we determine values for the λ_{zero} points: 421.075(2) and 423.018(7) nm.

We have presented the first experimental measurement of the $5s$-$6p$ dipole transition matrix elements in Rb. Our technique of measuring the relative light shift near λ_{zero} is applicable to many important atoms. At a minimum, such measurements constrain matrix elements and provide benchmarks needed for atomic theory. Additionally, applying our measurement technique to metastable states, such as the $^3P_0$ clock state of Yb or Sr, could provide information about excited-excited state matrix elements.

*cherold@umd.edu

[1] K. Beloy, J. A. Sherman, N. D. Lemke, N. Hinkley, C. W. Oates, and A. D. Ludlow, arXiv:1208.0552v1.

[2] J. A. Sherman, N. D. Lemke, N. Hinkley, M. Pizzocaro, R. W. Fox, A. D. Ludlow, and C. W. Oates, Phys. Rev. Lett. **108,** 153002 (2012).

[3] S. G. Porsev, A. D. Ludlow, M. M. Boyd, and J. Ye, Phys. Rev. A **78,** 032508 (2008).

[4] S. G. Porsev, K. Beloy, and A. Derevianko, Phys. Rev. Lett. **102,** 181601 (2009).

[5] A. A. Vasilyev, I. M. Savukov, M. S. Safronova, and H. G. Berry, Phys. Rev. A **66,** 020101 (2002).

[6] M. S. Safronova, U. I. Safronova, and C. W. Clark, Phys. Rev. A **86,** 042505 (2012).

[7] A. V. Gorshkov, A. M. Rey, A. J. Daley, M. M. Boyd, J. Ye, P. Zoller, and M. D. Lukin, Phys. Rev. Lett. **102,** 110503 (2009).

[8] M. Saffman and T. G. Walker, Phys. Rev. A **72,** 022347 (2005).

[9] H. P. Summers, N. R. Badnell, M. G. O'Mullane, A. D. Whiteford, R. Bingham, B. J. Kellett, J. Lang, K. H. Behringer, U. Fantz, K.-D. Zastrow, S. D. Loch, M. S. Pindzola, D. C. Griffin, and C. P. Ballance, Plasma Phys. Controlled Fusion **44,** B323 (2002).

[10] D. A. Verner, E. M. Verner, and G. J. Ferland, At. Data Nucl. Data Tables **64,** 1 (1996).

[11] J. C. Pickering, R. Blackwell-Whitehead, A. P. Thorne, M. Ruffoni, and C. E. Holmes, Can. J. Phys. **89,** 387 (2011).

[12] M. S. Safronova, M. G. Kozlov, and C. W. Clark, Phys. Rev. Lett. **107,** 143006 (2011).

[13] S. G. Porsev and A. Derevianko, Phys. Rev. A **74,** 020502 (2006).

[14] K. Aikawa, A. Frisch, M. Mark, S. Baier, A. Rietzler, R. Grimm, and F. Ferlaino, Phys. Rev. Lett. **108,** 210401 (2012).

[15] M. Lu, N. Q. Burdick, and B. L. Lev, Phys. Rev. Lett. **108,** 215301 (2012).

[16] M. Saffman and K. Mølmer, Phys. Rev. A **78,** 012336 (2008).

[17] N. Bouloufa, A. Crubellier, and O. Dulieu, Phys. Scr. **T134,** 014014 (2009).

[18] E. Gomez, S. Aubin, L. A. Orozco, and G. D. Sprouse, J. Opt. Soc. Am. B **21,** 2058 (2004).

[19] J. A. Sherman, T. W. Koerber, A. Markhotok, W. Nagourney, and E. N. Fortson, Phys. Rev. Lett. **94,** 243001 (2005).

[20] J. A. Sherman, A. Andalkar, W. Nagourney, and E. N. Fortson, Phys. Rev. A **78,** 052514 (2008).

[21] B. Sahoo, L. Wansbeek, K. Jungmann, and R. Timmermans, Phys. Rev. A **79,** 052512 (2009).

[22] B. Arora, M. S. Safronova, and C. W. Clark, Phys. Rev. A **84,** 043401 (2011).

[23] These are the "tune-out" wavelengths proposed for species-selective traps by L. J. LeBlanc and J. H. Thywissen, Phys. Rev. A **75,** 053612 (2007).

[24] M. Takamoto, F.-L. Hong, R. Higashi, and H. Katori, Nature (London) **435,** 321 (2005).

[25] Y.-J. Lin, A. R. Perry, R. L. Compton, I. B. Spielman, and J. V. Porto, Phys. Rev. A **79,** 063631 (2009).

[26] A. Shiner, A. Madej, P. Dubé, and J. Bernard, Appl. Phys. B **89,** 595 (2007).

[27] The vector light shift is identically zero, while the tensor shift is less than 3×10^{-5} times the scalar shift over the range of our measurements. Additionally, the hyperpolarizability (proportional to intensity squared) is at the 10^{-7} level.

[28] I. H. Deutsch and P. S. Jessen, Opt. Commun. **283,** 681 (2010).

[29] F. M. Izrailev and D. L. Shepelyanskii, Theor. Math. Phys. **43,** 553 (1980).

[30] F. L. Moore, J. C. Robinson, C. F. Bharucha, B. Sundaram, and M. G. Raizen, Phys. Rev. Lett. **75,** 4598 (1995).

[31] S. Wu, Y.-J. Wang, Q. Diot, and M. Prentiss, Phys. Rev. A **71,** 043602 (2005).

[32] L. Deng, E. W. Hagley, J. Denschlag, J. E. Simsarian, M. Edwards, C. W. Clark, K. Helmerson, S. L. Rolston, and W. D. Phillips, Phys. Rev. Lett. **83,** 5407 (1999).

[33] We account for the exact precession period numerically when determining the lattice depth.

[34] Some points exhibited decreased diffraction, correlated with the condensate position in each image, due to residual condensate motion. Thus we excluded the 22% of images where the condensate was more than 15 μm from the average position for each data set. The extracted matrix elements are insensitive to the exclusion value.

[35] U. Volz and H. Schmoranzer, Phys. Scr. **T65,** 48 (1996).

[36] See Supplemental Material at http://link.aps.org/supplemental/10.1103/PhysRevLett.109.243003 for a description of theoretical methods and improved results.

[37] That reduced χ^2 for the fits in Fig. 4 is larger than 1 is accounted for by the additional uncertainty in alignment drift, which we expect also explains the disparity between S and P fits; rescaling the statistical uncertainty to give a reduced χ^2 of 1 produces similar total uncertainty.